Journal of Power Sources 229 (2013) 229–233

Contents lists available at SciVerse ScienceDirect

Journal of Power Sources

journal homepage: www.elsevier.com/locate/jpowsour

Short communication

Hierarchical SiO_x nanoconifers for Li-ion battery anodes with structural stability and kinetic enhancement

Kyeongse Song [b,1], Sunyoung Yoo [c,1], Kibum Kang [a], Hoseok Heo [d], Yong-Mook Kang [b,**], Moon-Ho Jo [a,*]

[a] Department of Materials Science and Engineering, Yonsei University, Seongsan-No 262, Seodaemun-Gu, Seoul 120-749, Republic of Korea
[b] Department of Chemistry, Dongguk University-Seoul, Seoul 100-715, Republic of Korea
[c] Department of Materials Science and Engineering, Pohang University of Science and Technology (POSTECH), Pohang 790-784, Republic of Korea
[d] Division of Advanced Materials Science, Pohang University of Science and Technology (POSTECH), Pohang 790-784, Republic of Korea

HIGHLIGHTS

- The SiO_x nanoconifers were synthesized through a simple thermal evaporation process.
- SiO_x nanoconifers/$NiSi_x$ NW heterostructures displays enhanced anodic performances over bare SiO_x anodes.
- This improvement is attributed to the structural and kinetic stability.

GRAPHICAL ABSTRACT

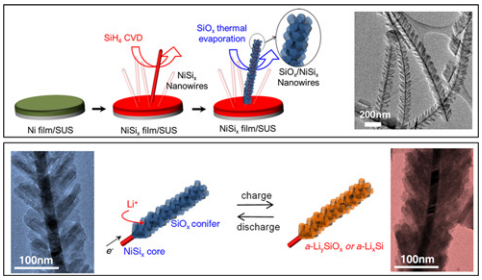

ARTICLE INFO

Article history:
Received 12 October 2012
Received in revised form
30 November 2012
Accepted 1 December 2012
Available online 12 December 2012

Keywords:
Silicon oxide
Li rechargeable battery
Anode
Nanoconifer
Nanowire
Thermal evaporation

ABSTRACT

Silicon sub-oxides, SiO_x ($0 < x < 1$) can be regarded as a promising anode material for high performance Li-ion batteries for its unique electrochemical reactions to Li. We designed and synthesized the columnar-shape SiO_x nanoconifers ($0.9 < x < 1$), directly self-organized on metallic $NiSi_x$ nanowires (NWs) for its anodic use in Li rechargeable batteries. The half-cell incorporating SiO_x nanoconifers/$NiSi_x$ NW heterostructures displays good cyclic retention and rate capability, which are attributed to the structural and kinetic stability of the hierarchical SiO_x nanoconifers rigidly supported by metallic $NiSi_x$ core NWs by providing a reversible electrochemical route with a lower activation energy.

1. Introduction

Lithium rechargeable batteries are efficient chemical-to-electrical energy conversion systems with eco-friendliness and sustainability [1–8]. Therein, the choice of appropriate electrode materials and their architectures, with which all the electrochemical entities must be optimally coordinated at the interfaces, largely determine their capacity and power characteristics [9–13]. Recently one-dimensional Si-based nanostructures have been

* Corresponding author. Tel.: +82 2 2123 5842; fax: +82 2 2123 5375.
** Corresponding author. Tel.: +82 2 2260 8674.
E-mail addresses: dake1234@dongguk.edu (Y.-M. Kang), mhjo@yonsei.ac.kr (M.-H. Jo).
[1] Equal contributors.

0378-7753/$ – see front matter © 2012 Elsevier B.V. All rights reserved.
http://dx.doi.org/10.1016/j.jpowsour.2012.12.002

extensively investigated as a next-generation anode material, mainly due to (1) the highest achievable, ever known, capacity of Si up to 4200 $mAhg^{-1}$ by the $Li_{4.4}Si$ intermetallic compound formation, and (2) their affordable accommodation of large volume-changes upon lithiation/delithiation and (3) the efficient charge collection capability [14–19]. Yet, pure Si nanoparticles or nanowires exhibit cyclic degradation in their cell capacity, particularly at the high charging/discharging rate, thus limiting their integration into the high power cells. In this regard, Si sub-oxides (SiO_x, $0 < x < 2$) may offer a practical solution as new anode materials, where the un-stoichiometric oxygen coordinations can provide an alternative electrochemical route, ensuing a marginal volume change with a potentially lower activation energy. Here, the responsible electrochemical reactions during the charge/discharge processes involve the conversion of SiO_x to the mixture of Si, lithium oxides and lithium silicates, as below.

$$SiO_x + yLi \leftrightarrow Si + Li_yO_x \quad (1)$$

$$xLi + Si \leftrightarrow Li_xSi \quad (2)$$

$$yLi + SiO_x \leftrightarrow Li_ySiO_x \quad (3)$$

Earlier, Yang et al. reported that the oxygen concentration in SiO_x particles influences cyclic reversibility and maximum capacity. Therein, $SiO_{0.8}$ and $SiO_{1.1}$ nanoparticles retain 40% and 93% of the initial discharge capacity after 25th cycle, respectively. Meanwhile, the discharge capacities of $SiO_{0.8}$ and $SiO_{1.1}$ nanoparticles are each 1700 $mAhg^{-1}$ and 750 $mAhg^{-1}$. It means that lower oxygen contents in SiO_x results in higher specific capacity with poor cycleability, whereas higher oxygen contents involve higher capacity retention in spite of a little structural instability [20]. Wang et al. demonstrated that Si/SiO_x nanocomposite with core–shell structure displays the superior reversibility that 70% of the initial capacity (1100 $mAhg^{-1}$) is maintained even after 50th cycle and the highest Coulombic efficiency among Si-based materials thanks to its structural feature [21]. These observations strongly suggest that the choice of SiO_x can provide a way to accommodate the relatively large volume expansion with higher interfacial stability for the extended cycle life. Nevertheless, the fundamental drawback of SiO_x anodes is its intrinsically poor electronic conductivity, inevitably limiting the required rate capability upon cycling. For this reason, many researchers have tried to develop conductive composite based on SiO_x nanoparticles through its disproportion [22] or carbon coating [23]. Here, we demonstrate an advanced SiO_x anode architecture, where the active SiO_x is self-assembled on metallic $NiSi_x$ nanowires (NWs) to form hierarchical SiO_x nanoconifers by a simple chemical vapor deposition (CVD) process, for the improved cyclic reversibility and enhanced kinetics. We show that SiO_x nanoconifers on $NiSi_x$ NWs act as an active element for alloying/de-alloying with Li ions with substantially higher surface areas, and the metallic $NiSi_x$ NWs serve both as efficient electron transport pathway and as rigid mechanical supports. It is evident that this unique hierarchical SiO_x nanoconifer composite maintains their original shapes during the extended cycling resultantly showing enhanced cycleability and rate capability thanks to its structural stability coming from heterostructure.

2. Experimental

2.1. Synthesis of hierarchical SiO_x nanoconifers

Fig. 1(a) schematically illustrates the growth sequence of SiO_x nanoconifers supported by metallic $NiSi_x$ NWs ($SiO_x/NiSi_x$ NWs) by a CVD process. We first begin with the growth of $NiSi_x$ NWs via 50 Torr of SiH_4 CVD (10% diluted SiH_4 in H_2) at 420 °C on Ni/stainless steel (SUS) substrates of a circular shape disk in 15 mm diameter [24,25]. Our $NiSi_x$ NWs exhibit typical metallic behaviors with its resistivity on the order of a few hundred μΩ cm at 300 K [26,27]. Then SiO_x overlayers are deposited on $NiSi_x$ NW arrays using thermal evaporation of silicon monoxide powder (SiO, Aldrich) in the high vacuum (under 10^{-6} Torr) cold wall chamber. The oxygen contents (x) in the final SiO_x products are optimized to be ranged between 0.9 and 1. The weights of the deposited SiO_x and $NiSi_x$ were averagely 0.122 mg and 0.125 mg, respectively.

2.2. Structure characterization

The morphology and microstructure of lamellar SiO_x and $NiSi_x$ nanowire were characterized by field emission scanning electron microscopy (FE-SEM, JEOL JSM-7401F) on SEI mode at 10 kV, and transmission electron microscopy (TEM, JEOL JEM-2100F with Cs Corrector on STEM) at NCNT. The chemical structure analysis was performed by X-ray photoelectron spectroscopy (XPS) (VG SCIENTIFIC ESCALAB 220i) spectrometer using focused mono-chromated Mg Kα radiation to probe the surface of the SiO_x.

2.3. Electrochemical experiments

Commercially provided SiO_x bulk was used as reference sample for the electrochemical comparison with $SiO_x/NiSi_x$ NW. SiO_x bulk was mixed with acetylene black (AB) and binder, poly(vinylidene fluoride), at a weight ratio of 9:1:1, respectively, in a solvent (N-methyl-2-pyrrolidone). The slurry was uniformly pasted on Cu foil. The prepared electrode sheets were dried at 120 °C in a vacuum oven and pressed under a pressure of approximately 2000 psi. The $SiO_x/NiSi_x$ NW anodes were incorporated into a coin-type half cell (CR2016 coin-type) without binders or conducting carbon. Both cells were assembled in an argon-filled glove box for electrochemical characterization. The electrolyte was 1 M $LiPF_6$ in a 1:1 mixture of ethylene carbonate and dimethyl carbonate. Li metal foil was used as the counter and reference electrode. The monolayer polypropylene membrane (Celgard 2400) was adopted as a separator. The cell was galvanostatically charged and discharged at a current density of 150 mAg^{-1} over a range of 0.01 V–1.20 V for the first cycle. Then, for the remaining cycles, it was charged/discharged at 300 mAg^{-1}.

3. Results and discussion

Fig. 1(b) shows the representative transmission electron microscope (TEM) image and scanning electron microscope (SEM) image of $SiO_x/NiSi_x$ NWs, where their average length and diameter are 5 μm and 170 nm with the 30 nm thick $NiSi_x$ core. Notably, SiO_x shells do not conformally deposit on the $NiSi_x$ core NWs and instead it forms a conifer shape where periodic SiO_x columns are self-assembled with a high packing density, as shown in Fig. 1(b)–(c). This unique columnar structure formation can be understood as a combination of the limited numbers of nucleation sites on $NiSi_x$ NWs and the low mobility of the adatoms on the cold substrates during thermal evaporation of SiO_x [28,29].

Elemental analyses of $SiO_x/NiSi_x$ NWs were carried out with a scanning TEM as shown in Fig. 1(c). High-angle annular dark field (HAADF) images, where the intensity of HAADF is roughly proportional to the square of atomic numbers, indicate that the composition of the shell region and core region in $SiO_x/NiSi_x$ NWs are clearly discernable. The corresponding energy dispersive X-ray spectroscopy (EDX) color maps also present that the elemental distribution of Ni is locally confined in the core region within the

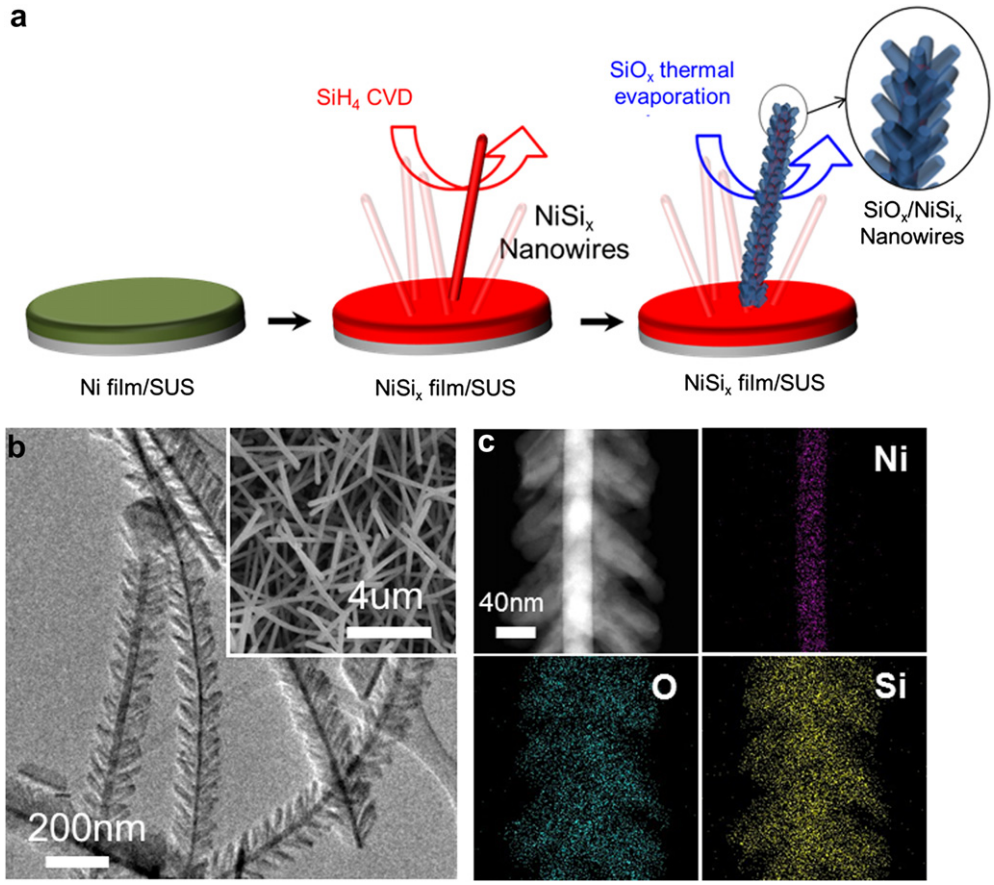

Fig. 1. (a) The schematics of SiO_x nanoconifer on $NiSi_x$ NWs growth process. (b) Low resolution TEM image of $SiO_x/NiSi_x$ NWs. The inset shows plan-view SEM image of $SiO_x/NiSi_x$ NW arrays grown on SUS substrate. (c) STEM HAADF images and EDX elemental color map of an individual $SiO_x/NiSi_x$ NWs.

instrumental resolution, whereas Si and O are well distributed all over the shell region.

Oxidation states of the $SiO_x/NiSi_x$ NWs are determined by X-ray photoelectron spectroscopy (XPS), as shown in Fig. 2. We have taken Si 2p spectra of Si NWs and SiO_2 powders as the references. Apparently, the Si 2p peak in SiO_x is located between those in Si (99.3 eV) and SiO_2 (103.4 eV), where the deconvoluted feature is comprised all of the variable $Si(-O)_n$ (n = 1,2,3,4) bonding as

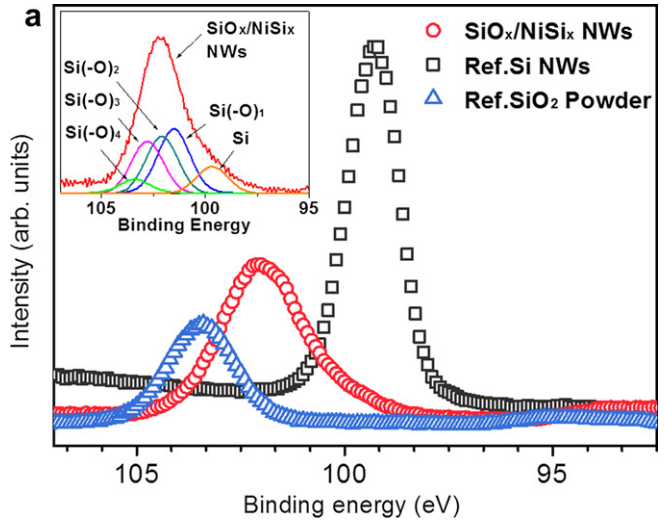

Fig. 2. (a) Si 2p XPS spectra of SiO_x shell for chemical structure analysis. (Note that the each XPS spectra have been normalized to c–c bonding, C1s 284 eV).

described in inset of Fig. 2. We extract the average oxygen contents, x, of SiO_x nanoconifers to be 0.9–1. It is reported that SiO_x anodes display an optimum capacity with cycle performance for $x \sim 1$ [20,30], due to a balance between the affordable accommodation of the inherent volume expansion by Li–Si reactions and the irreversible reaction for the detrimental Li_2O phase formation [14,31,32]. In this regard, the oxygen content of 0.9–1 in our SiO_x nanoconifers holds promises for the anodic use in terms of cyclic retention as well as specific capacity.

Fig. 3 displays the charge/discharge performance of SiO_x nanoconifers, measured over 100 cycles, including the specific capacity, Coulombic efficiency and the rate capability. Considering that the $NiSi_x$ core does not participate in charge/discharge reaction, SiO_x nanoconifers seem to show the maximum capacity almost reaching the theoretical capacity of Si besides the irreversible capacity induced by the formation of Li_2O and lithium silicates, as well as good cyclic retention. Meanwhile, SiO_x bulk exhibits very low capacity around 500–600 $mAhg^{-1}$, and its capacity drastically drops in a few cycles. The first discharge and charge capacities of SiO_x nanoconifers are measured to be 4058 and 1737 $mAhg^{-1}$ at the current density of 150 mAg^{-1}, which produce the irreversible capacity loss of 57% at the very first cycle. We speculate that this initial loss comes from the reaction of the amorphous SiO_x with Li ions, forming some irreversibly lithiated phases, such as inactive lithium silicates or Li_2O. Because Li_2O or lithium silicate have shown little electrochemical activity due to their high thermodynamic stability, the formation of theses phases can result in low initial coulombic efficiency as shown in Fig. 3(a). Nevertheless, the formation of these inactive phases in the open structures of the amorphous SiO_x may contribute to the improved cyclic retention by

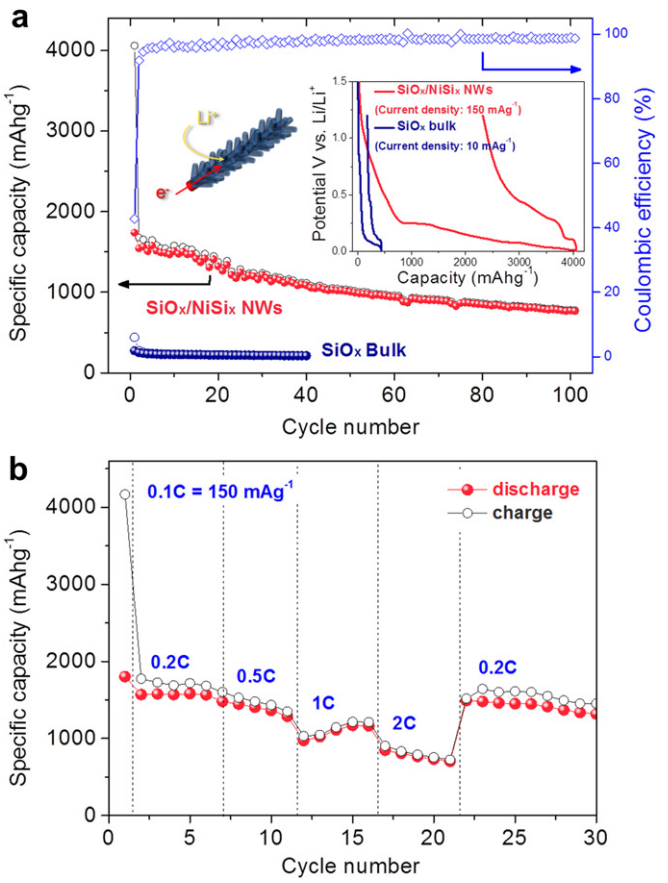

Fig. 3. (a) Electrochemical cycle life time including the coulombic efficiency and the specific capacity vs the charge/discharge cycle number of $SiO_x/NiSi_x$ NWs (inset: the galvanostatic charge–discharge curves between 0.01 and 1.2 V). (b) Plots of discharge retention versus cycle number at different C rates.

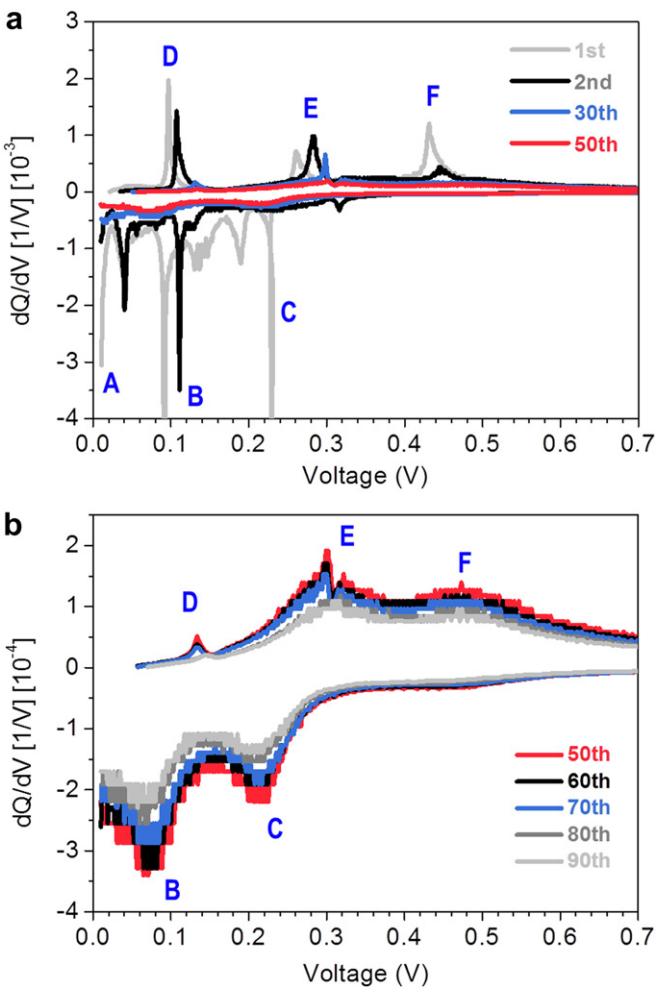

Fig. 4. (a) The differential capacity plots of 1, 2, 30 and 50th cycle for $SiO_x/NiSi_x$ NWs (b) and its 50, 60, 70, 80 and 90th cycle.

alleviating the severe volume expansion, as a cushioning media, as further discussed below. After the first cycle, the SiO_x nanoconifer cell shows very high coulombic efficiency over 97% for the subsequent cycles. This may be due to the presence of metallic $NiSi_x$ cores, which serve as the efficient charge transport pathway from/to insulating SiO_x phases. After 20 cycles, the capacity is measured to be ~1375 $mAhg^{-1}$, which correspond to ~80% of the initial capacity. Then, its capacity is gradually degraded to about 800 $mAhg^{-1}$ up to the 100th cycle. This gradual degradation after the 20th cycle is often observed in the anode of Si-based materials, due to the interfacial instability with the additive-free electrolytes in use, which can be further reduced by an electrolyte modification [33]. The rate capability was tested by varying the galvanostatic current density from 0.2C to 2C for the charge/discharge process, as shown in Fig. 3(b). It shows an excellent retention even at the 10 times higher current density than one in the initial condition, demonstrating enhanced kinetics of SiO_x nanoconifers on metallic cores compared to pure SiO_x particles [34]. The gradual capacity increase of SiO_x conifers at 1C can be attributed to the change of activation energy for the chemical reaction between Li^+ and SiO_x conifers.

In order to identify electrochemical routes [9,22,25,34–36] of Si species in our SiO_x nanoconifers, we analyze the differential capacity plots (dQ/dV vs. V), obtained for the 1st, 2nd, 30th, and 50th cycle. Possible intermetallic compounds from the reactions between SiO_x and Li include lithium oxides, lithium silicates, and lithium silicides. During the initial lithiation, $SiO_x/NiSi_x$ NWs produce several reduction peaks corresponding to the formation of typical intermetallic compounds marked by *A*, *B*, and *C* in Fig. 4(a). The peak *C* at 220 mV and the *B* peak at 90 mV are attributed to the phase transition between amorphous Li_xSi phases, while the *A* peak at 40 mV can be assigned to the phase transition from amorphous lithium silicides to a crystalline $Li_{15}Si_4$ phase [24,25].

Other weak reduction peaks near ~0 V [23] and ~310 mV [33] are from the solid–solution reactions between Li and SiO_x. We do not observe any evidence for the formation of either SEI phases or Li_2O, which may be overridden by the lower energy formation of lithium silicates. It is in fact consistent with the presence of the first oxidation peak at 100 mV during the delithiation process, marked by *D*, which corresponds to the dissociation of lithium silicates. A narrow peak at 250 mV, marked by *E*, can be assigned to the dissociation of a-$Li_{x+y}Si$ to Li_xSi or a-Si, while the peak at 450 mV, marked by *F*, results from the decomposition of c-$Li_{15}Si_4$ to a-Li_xSi or a-Si [24,25,37,38]. Small separation between reduction and oxidation peaks assigned to lithium silicates indicates that Li ions are weakly bonded to SiO_x rather than to Si, and thus Li ion transport can be accelerated by the preferential reaction of Li ions with SiO_x [39,40]. Differential capacity plots obtained after 50th, 60th, 70th, 80th and 90th cycle in Fig. 4(b) suggest that SiO_x nanoconifers undergo the phase transitions between amorphous lithiated phases and amorphous delithiated phases including a-Li_xSi/a-Si pairs and a-Li_ySiO_x/a-SiO_x pairs in Eqs. (2) and (3) [9,34,35]. Then, these reversible reaction paths with lower formation energy in SiO_x nanoconifer may be one of the main reasons for the enhanced cyclic retention and rate capability in Fig. 3.

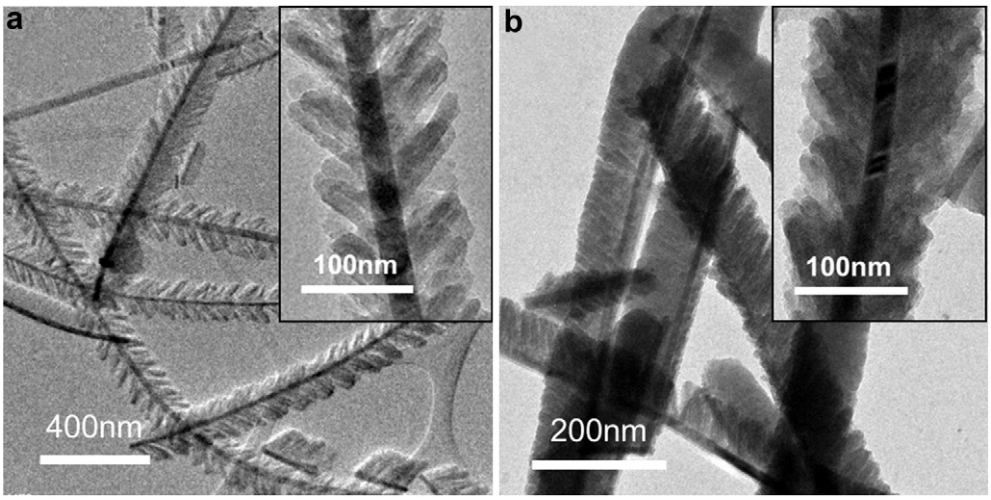

Fig. 5. (a) TEM images of as-grown $SiO_x/NiSi_x$ NWs and (b) the 100th lithiated $SiO_x/NiSi_x$ NWs. Insets show individual $SiO_x/NiSi_x$ NWs in more details.

Fig. 5 shows the TEM images of as-grown $SiO_x/NiSi_x$ NWs and those after the 100th lithiation. Remarkably, the original shape of SiO_x conifer shells and $NiSi_x$ core NWs is almost intact after repeated cycles, except for the local densification due to lithiation. This strongly suggests that our heterostructures undergo stably endurable volume change upon the repeated lithiation/delithiation as aforementioned, and also consistent with theoretical prediction [41]. Supposing that 9 at% pure Si atoms based on XPS elemental analyses participate in the partial Li_xSi phase formation, the expected volume expansion of SiO_x columns comes to 10–20 nm in diameter. Nevertheless, the regularly spaced voids among individual SiO_x columns must accommodate its volume expansion. It can also reduce Li ion diffusion pathways through facile electrolyte penetration. In this regard, the columnar shape provides great advantages in viewpoint of structural stability as well as enhanced kinetics for the anodic use of $SiO_x/NiSi_x$ NWs.

4. Conclusion

We synthesized SiO_x nanoconifers on $NiSi_x$ core NWs by thermal evaporation coupled with SiH_4 chemical vapor deposition process. SiO_x nanoconifer forms its own characteristic columnar shape on $NiSi_x$ NWs in a self-organized manner, where its oxygen composition, x, ranged in 0.9–1 for its anodic use. The half-cell incorporating $SiO_x/NiSi_x$ NWs displays good cyclic retention and rate capability attributed to the structural and kinetic stability of the hierarchical SiO_x conifers rigidly attached to metallic $NiSi_x$ core NWs.

Acknowledgements

Moon-Ho Jo acknowledges Basic Science Research Program (2012-0005650 and 2012-0000623), Global Frontier Research Program (2011–0031639), Nano Original & Fundamental Technology R&D Program (20120006217) through the NRF funded by the MEST. Yong-Mook Kang acknowledges the Basic Science Research Program (20090072972) and (NRF-2010-C1AAA001-0029018) through the NRF of Korea funded by the MEST, and the Fundamental R&D Program for Technology of World Premier Materials funded by the Ministry of Knowledge Economy (10037918).

References

[1] J.-M. Tarascon, M. Armand, Nature 414 (2001) 359.
[2] P.G. Bruce, B. Scrosati, J.-M. Tarascon, Angew. Chem. 47 (2008) 2930.
[3] P. Poizot, S. Laruelle, S. Grugeon, L. Dupont, J.-M. Tarascon, Nature 407 (2000) 496.
[4] S.Y. Chung, J.T. Bloking, Y.-M. Chiang, Nat. Mater. 1 (2002) 123.
[5] J.Y. Song, Y.Y. Wang, C.C. Wan, J. Power Sources 77 (1999) 183.
[6] D. Wang, D. Choi, J. Li, Z. Yang, Z. Nie, R. Kou, D. Hu, C. Wang, L.V. Saraf, J. Zhang, I.A. Aksay, J. Liu, ACS Nano 3 (2009) 907.
[7] D. Deng, J.Y. Lee, Chem. Mater. 20 (2008) 1841.
[8] W. Wang, P.N. Kumta, ACS Nano 4 (2010) 2233.
[9] Y.M. Kang, S.M. Lee, S.J. Kim, G.J. Jeong, M.S. Sung, W.U. Choi, S.S. Kim, Electrochem. Commun. 9 (2007) 959.
[10] C.K. Chan, X.F. Zhang, Y. Cui, Nano Lett. 8 (2008) 307.
[11] C.K. Chan, H. Peng, G. Liu, K. McIlwrath, X.F. Zhang, R.A. Huggins, Y. Cui, Nat. Nanotechnol. 3 (2008) 31.
[12] R.A. Huggins, J. Power Sources 81 (1999) 13.
[13] G. Derrien, J. Hassoun, S. Panero, B. Scrosati, Adv. Mater. 19 (2007) 2336.
[14] K. Kim, J.H. Park, S.G. Doo, T. Kim, Thin Solid Films 518 (2010) 6547.
[15] H. Yoo, J.I. Lee, H. Kim, J.P. Lee, J. Cho, S. Park, Nano Lett. 11 (2011) 4324.
[16] M. Miyachi, H. Yamamoto, H. Kawai, T. Ohta, M. Shirakata, J. Electrochem. Soc. 152 (2005) A2089.
[17] Y. Liu, J. Yang, N. Imanishi, A. Hirano, Y. Takeda, O. Yamamoto, J. Power Sources 146 (2005) 376.
[18] L. Su, Z. Zhou, M. Ren, Chem. Commun. 46 (2010) 2590.
[19] H. Wu, G. Chan, J.W. Choi, I. Ryu, Y. Yao, M.T. McDowell, S.W. Lee, A. Jackson, Y. Yang, L. Hu, Y. Cui, Nat. Nanotechnol. 7 (2012) 310.
[20] J. Yang, Y. Takeda, N. Imanishi, C. Capiglia, J.Y. Xie, O. Yamanoto, Solid State Ionics 152 (2002) 125.
[21] J. Wang, H. Zhao, J. He, C. Wang, J. Wang, J. Power Sources 196 (2011) 4811.
[22] Y.-S. Hu, R. Demir-Cakan, M.-M. Titirici, J.-O. Müller, R. Schlögl, M. Antonietti, J. Maier, Angew. Chem. 47 (2008) 1645.
[23] T. Zhang, J. Gao, H.P. Zhang, L.C. Yang, Y.P. Wu, H.Q. Wu, Electrochem. Commun. 9 (2007) 886.
[24] K. Kang, H.-S. Lee, D.-W. Han, G.-S. Kim, D. Lee, G. Lee, Y.-M. Kang, M.-H. Jo, Appl. Phys. Lett. 96 (2010) 053110.
[25] K. Kang, K. Song, H. Heo, S. Yoo, G.-S. Kim, G. Lee, Y.-M. Kang, M.-H. Jo, Chem. Sci. 2 (2011) 1090.
[26] K. Kang, S.-K. Kim, C.-J. Kim, M.-H. Jo, Nano Lett. 8 (2008) 431.
[27] C.-J. Kim, K. Kang, Y.S. Woo, K.-G. Ryu, H. Moon, J.-M. Kim, D.-S. Zang, M.-H. Jo, Adv. Mater. 19 (2007) 3637.
[28] T. Karabacak, G.-C. Wang, T.-M. Lu, J. Vac. Sci. Technol. A 22 (4) (2004) 1778.
[29] A.G. Dirks, H.J. Leamy, Thin Solid Films 47 (1997) 219.
[30] M. Miyachi, H. Yamamoto, H. Kawai, T. Ohto, M. Shirakata, J. Electrochem. Soc. 10 (2005) A2089.
[31] C.-H. Doh, A. Veluchamy, D.-J. Lee, J.-H. Lee, B.-S. Jin, S.-I. Moon, C.-W. Park, D.-W. Kim, Bull. Korean Chem. Soc. 31 (2010) 1257.
[32] C.-M. Park, W. Choi, Y. Hwa, J.-H. Kim, G. Jeong, H.-J. Sohn, J. Mater. Chem. 20 (2010) 4854.
[33] N.-S. Choi, K.H. Yew, K.Y. Lee, M. Sung, H. Kim, S.-S. Kim, J. Power Sources 161 (2006) 1254.
[34] Y.-M. Kang, S.-B. Suh, Y.-S. Kim, Inorg. Chem. 48 (2009) 11631.
[35] Y.-M. Kang, J.-Y. Go, S.-M. Lee, W.-U. Choi, Electrochem. Commun. 9 (2007) 1276.
[36] M.N. Obrovac, L. Christensen, Electrochem. Solid-State Lett. 7 (2004) A93.
[37] P.R. Abel, Y.M. Lin, H. Celio, A. Heller, C.B. Mullins, ACS Nano 6 (2012) 2506.
[38] W.R. Liu, Y.C. Yen, H.C. Wu, M. Winter, N.L. Wu, J. Appl. Electrochem. 39 (2009) 1643.
[39] G.V. Gibbs, M.M. Hamil, S.J. Louisnathan, Am. Mineral. 57 (1972) 1578.
[40] A. Bongiorno, A. Pasquarello, Phys. Rev. B 62 (2000) 24.
[41] C.-H. Doh, A. Veluchamy, M.-W. Oh, B.-C. Han, J. Electro. Sci. Tech. 2 (2011) 146.